NRIAG Journal of Astronomy and Geophysics (2015) 4, 25–31

National Research Institute of Astronomy and Geophysics

NRIAG Journal of Astronomy and Geophysics

www.elsevier.com/locate/nrjag

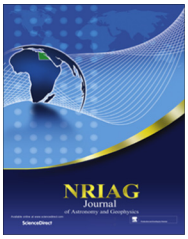

Dynamical study of low Earth orbit debris collision avoidance using ground based laser

N.S. Khalifa *

Mathematics Department, Deanship of Preparatory Year – Girls Branch, Hail University, Hail, Saudi Arabia
National Research Institute of Astronomy and Geophysics (NRIAG), Cairo, Egypt

Received 4 January 2014; revised 27 January 2015; accepted 6 February 2015
Available online 30 April 2015

KEYWORDS

Space debris;
Low Earth orbit;
Laser force;
Geocentric coordinate system;
Perturbations of orbital elements;
Collision avoidance

Abstract The objective of this paper was to investigate the orbital velocity changes due to the effect of ground based laser force. The resulting perturbations of semi-major axis, miss distance and collision probability of two approaching objects are studied. The analytical model is applied for low Earth orbit debris of different eccentricities and area to mass ratio and the numerical test shows that laser of medium power ~5 kW can perform a small change $\Delta\overline{V}$ of an average magnitude of 0.2 cm/s which can be accumulated over time to be about 3 cm/day. Moreover, it is confirmed that applying laser $\Delta\overline{V}$ results in decreasing collision probability and increasing miss distance in order to avoid collision.

1. Introduction

During the recent years, functional satellites are threatened by enormous number of space debris which increases dramatically as the use of space expands. Radar and optical surveillance systems, as well as direct impact measurements, show that there are a huge number of debris in low Earth orbits of about 1–10 cm size. In frame of orbital debris removal, several broad research efforts have been performed. The majority of these researches were based on vaporization or ablation of these small objects using different ground based laser systems in order to permit debris re-entry. However, building and operating of such systems are the most cost effective way to mitigate the debris problem (Phipps et al., 2012; Campbell et al., 2000; Choi and Pappa, 2012).

In comparison of those schemes that aimed to de-orbiting debris using laser powers, laser collision avoidance maneuver requires much less force and less sophisticated laser systems. The application of small change ΔV results in lowering or rising of semi-major axis and orbital period allowing rapid along-track displacement to grow over time. This causes the two approaching objects to miss each other in time even if the orbital elements remain essential unchanged Stupl et al. (2010).

Many authors studied the feasibility of using a medium power laser of about 5–10 kW to avoid fraction of collisions in low Earth orbit (Stupl et al., 2010; Mason et al., 2011).

* Address: National Research Institute of Astronomy and Geophysics (NRIAG), Cairo, Egypt.
Peer review under responsibility of National Research Institute of Astronomy and Geophysics.

Production and hosting by Elsevier

http://dx.doi.org/10.1016/j.nrjag.2015.02.001

The main issue of this paper is to represent a dynamical study of using ground based laser as debris collision avoidance tool. This work is organized as follows: Section 2 represents the analytical modeling of the problem which includes the formulation of light force and orbital velocity changes using a geocentric equatorial coordinate system in addition to miss distance and collision probability. Section 3 represents the numerical applications and the general conclusion.

2. Laser collision avoidance

2.1. Laser beam propagation

For standard atmospheric conditions, only linear mechanism of laser atmospheric interactions is considered. Atmospheric turbulences are countered by using the adaptive optics and technical capabilities of the laser system. Based on the previous postulates, the laser intensity delivered to the debris surface is determined using an analytical model in which laser intensity is proportional to the laser power and inversely to debris altitude and laser divergence. This laser intensity is given by El-Saftawy et al. (2007) and Khalifa (2009):

$$S(\rho) = \frac{P}{\pi\theta^2\rho_{\text{debris}}^2}\text{Exp} - \left[\left[\frac{\sigma_{\text{scat}}^{\text{mol}}(0)h}{\sin(\phi)}\right]\left[1-\text{Exp}\left(-\frac{\rho\sin(\phi)}{h}\right)\right]+\sigma_{\text{scat}}^{\text{aer}}(\rho)\right], \tag{1}$$

where ρ_{debris} is the debris altitude, P is the laser power, θ is the beam divergence, ϕ is the elevation angle, $\sigma_{\text{scat}}^{\text{mol}}(0)$ is the molecule scattering coefficient at sea level, $\sigma_{\text{scat}}^{\text{aer}}$ is the aerosols scattering coefficient and h is the sea level altitude. ρ is considered to be the first 50 km of the Earth's atmosphere which is considered as the most effective on the beam propagation Danielson et al. (2003).

2.2. Laser force

The total radiant force exerted on a flat non-perfectly reflecting surface is given by Mc Innes Colin (1999):

$$\bar{f} = \frac{SA}{C}\psi\hat{m} \tag{2}$$

where

$$\psi = \left[4\rho'\beta\cos^4\eta + 2(1+\rho'\beta)\left(B_f\rho'(1-\beta)+\alpha'\frac{\varepsilon_f B_f-\varepsilon_b B_b}{\varepsilon_f+\varepsilon_b}\right)\cos^3\eta + \left\{\left(B_f\rho'(1-\beta)+\alpha'\frac{\varepsilon_f B_f-\varepsilon_b B_b}{\varepsilon_f+\varepsilon_b}\right)^2+(1-\rho'\beta)^2\right\}\cos^2\eta\right]^{1/2} \tag{3}$$

where $\hat{m}$ is a unit vector directed through the force direction, c is the speed of light and S is the radiation intensity at debris surface, η is the radiation incident angle on debris surface normal, β is debris surface specularity, ρ' is debris surface reflectivity, B_f and B_b are the non-Lambertian coefficient of front and back debris surfaces respectively, α' is debris absorption coefficient, and ε_f and ε_b are front and back debris surface emissivity, respectively. ψ can take a value from 1 to 2, where $\psi = 0$ means that the object is translucent, $\psi = 2$ means that all photons are reflected and for the object that absorbs all of the incident radiation $\psi = 1$.

For non-perfectly reflecting surfaces, The force vector, $\hat{m}$, is not directed normal to the surface. But, it inclines by an angle ϑ, known as the cone angle, to the incident direction, $\hat{\rho}_{\text{debris}}$. Then, force components in the incident direction will be:

$$\bar{f}_{\rho_{\text{debris}}} = \frac{SA}{C}\psi\cos\vartheta\hat{\rho}_{\text{debris}}. \tag{4}$$

2.3. Coordinate systems

The geocentric equatorial system is used with the unit vectors; $\hat{e}_x$ directed parallel to the Earth equatorial plane, $\hat{e}_y$ directed in the plane that contains the meridian of the sub-debris point and $\hat{e}_z$ directed normal to the equatorial plane. As shown in Fig. 1, the incident radiation vector, $\bar{\rho}_{\text{debris}}$, is given by:

$$\bar{\rho}_{\text{debris}} = \bar{r} - \bar{r}_E, \tag{5}$$

where $\bar{r}$ is debris position vector and $\bar{r}_E$ is the Earth radius vector (station coordinates). For an oblate Earth, the Earth radius vector is given by Escobal (1965):

$$\bar{r}_E = \begin{bmatrix} G_1\cos\varphi_g\cos\tau \\ G_1\cos\varphi_g\sin\tau \\ G_2\sin\varphi_g \end{bmatrix}, \tag{6}$$

with

$$G_1 = \frac{a_e}{\left(1-(2f_e'-f_e'^2)\sin^2\varphi_g\right)^{1/2}}+h, \qquad G_2 = \frac{a_e(1-f_e')^2}{\left(1-(2f_e'-f_e'^2)\sin^2\varphi_g\right)^{1/2}}+h, \tag{7}$$

where a_e is the Earth's Equatorial radius, f_e' is the Earth's flattening, φ_g is the geodetic latitude, h is the height above sea level and τ is the sidereal time.

The debris position vector, $\bar{r}$, in the geocentric coordinate system, is given by Escobal (1965):

$$\bar{r} = r\begin{pmatrix} \cos\Omega\cos(\omega+\upsilon)-\sin\Omega\sin(\omega+\upsilon)\cos i \\ \sin\Omega\cos(\omega+\upsilon)+\cos\Omega\sin(\omega+\upsilon)\cos i \\ \sin(\omega+\upsilon)\sin i \end{pmatrix}, \tag{8}$$

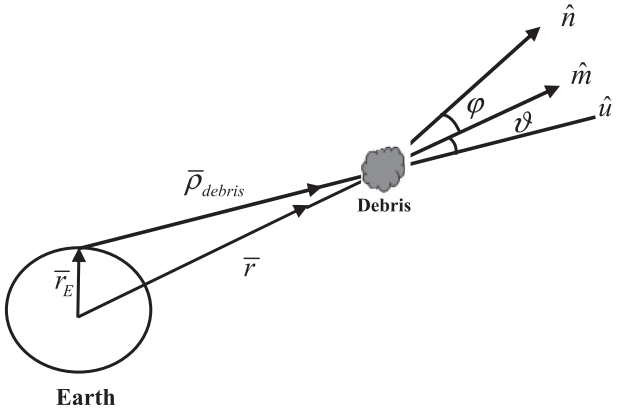

Figure 1 Ground based laser beam fires toward debris.

with

$$r = \frac{a(1-e^2)}{1+e\cos\upsilon},$$

where Ω is longitude of the ascending node, ω is argument of perigee, υ is the true anomaly, i is the inclination, a is the semi-major axis and e is the eccentricity. Using the geocentric coordinate system, the incident radiation vector is:

$$\bar{\rho}_{\text{debris}} = \rho_x\hat{e}_x + \rho_y\hat{e}_y + \rho_z\hat{e}_z \tag{9}$$

with

$$\rho_x = r(\cos\Omega\cos(\omega+\upsilon) - \sin\Omega\sin(\omega+\upsilon)\cos i) - G_1\cos\varphi_g\cos\theta, \tag{10}$$

$$\rho_y = r(\sin\Omega\cos(\omega+\upsilon) + \cos\Omega\sin(\omega+\upsilon)\cos i) - G_1\cos\varphi_g\sin\theta, \tag{11}$$

$$\rho_z = r\sin(\omega+\upsilon)\sin i - G_2\sin\varphi_g. \tag{12}$$

2.4. Laser perturbations

For high laser repetition rate, many laser shots fire toward the object over an interval of time. Consequently, the force can be considered as continuous function which can produce an orbital velocity change, $\Delta\overline{V}$, over an interval of time.

$$\left|\Delta\overline{V}\right| = \int_{t_o}^{t_1}\frac{|\bar{f}_\rho(t)|}{M}dt = \int_{t_o}^{t_1}|\bar{a}(t)|dt \tag{13}$$

The interval $(t_1 - t_o)$ is the exposure time where t_o and t_1 are the times of debris rising and setting. $\bar{a}(t)$ is the acceleration affecting on the debris motion due to laser force. At a given time, the acceleration experienced by debris of mass M is:

$$\bar{a} = \frac{\bar{f}_\rho}{M}. \tag{14}$$

The radial component of the disturbing acceleration, S is given by:

$$\begin{aligned} S &= \bar{a}\cdot\hat{r} \\ &= \frac{S\psi}{c\rho_{\text{debris}}^3}\frac{A}{M}\cos\vartheta[r - G_1\cos\varphi'(\cos(\theta'-\Omega)\cos(\omega+\upsilon) \\ &\quad + \sin(\theta'-\Omega)\sin(\omega+\upsilon)\cos i) + G_2\sin\varphi'\sin i\sin(\omega+\upsilon)], \end{aligned} \tag{15}$$

The tangential component of disturbing acceleration is given by:

$$T = \bar{a}\cdot(\widehat{H}\times\hat{r})$$

where $\widehat{H}$ is a unit vector in the direction of the angular momentum vector. It can be expressed as Escobal (1965):

$$\widehat{H} = \sin i\sin\Omega\hat{e}_x - \sin i\cos\Omega\hat{e}_y + \cos i\hat{e}_z, \tag{16}$$

$$\begin{aligned} T = \frac{S\psi}{c\rho_{\text{debris}}^3}\frac{A}{M}\cos\vartheta[&G_1\cos\varphi'(\cos(\theta'-\Omega)\sin(\omega+\upsilon) \\ &- \sin(\theta'-\Omega)\cos(\omega+\upsilon)\cos i) - G_2\sin\varphi'\sin i\sin(\omega+\upsilon)], \end{aligned} \tag{17}$$

The perpendicular component of disturbing acceleration is given by:

$$W = \bar{a}\cdot\widehat{H},$$

$$W = \frac{S\psi}{c\rho_{\text{debris}}^3}\frac{A}{M}\cos\vartheta[G_1\cos\varphi'\sin i\sin(\theta'-\Omega) - G_2\sin\varphi'\cos i]. \tag{18}$$

2.5. Laser collision avoidance

The laser disturbing acceleration results in perturbing debris semi-major axis a. For orbits of $e\neq0$ and $i\neq0$, these perturbations can be evaluated using the general perturbation equations of Roy (1978):

$$\dot{a} = \frac{2}{n\sqrt{1-e^2}}[T + Se\sin\upsilon + Te\cos\upsilon] \tag{19}$$

where n the orbital mean motion. This semi-major perturbation will result in a rapid along-track displacement which grows over time.

One fundamental aspect of this collision avoidance is the modeling of the relative dynamics of the two objects, the computation of the collision probability between two objects given their relative b-plane position and covariance matrices of along, normal and cross-track errors.

Consider two objects S_1 and S_2 experience a conjunction event with an expected miss distance r_m. Let us assume that a collision would take place whenever the following condition is verified Bombardelli et al. (2014) and Bombardelli (2014):

$$r_m = |\bar{r}_1 - \bar{r}_2| < S_A \tag{20}$$

where $\bar{r}_1$ and $\bar{r}_2$ are the randomly distributed positions of S_1 and S_2. S_A can be taken as the sum of the radii of the spherical envelopes centered at S_1 and S_2, respectively. The probability of collision between S_1 and S_2 can be written, in general terms, as the triple integral of the probability distribution function $f_{r_m}(r_m)$ of the relative position of S_1 with respect to S_2 over the volume swept by sphere of radius S_A centered at S_2:

$$P = \int_{\text{Vol}} f_{r_m}(r_m)dr_m \tag{21}$$

When the statistical distribution $f_r(r)$ is Gaussian it can be written as:

$$f_{r_m}(r_m) = \frac{\exp\left(-\frac{1}{2}(r_m - r_e)^T C_r^{-1}(r_m - r_e)\right)}{(2\pi)^{3/2}\sqrt{\det(C_r)}} \tag{22}$$

where r_e is the distance of closest approach, C_r is the covariance matrix of r_m, which corresponds to the sum of the individual covariance matrices of $\bar{r}_1$ and $\bar{r}_2$, expressed in the same orthonormal base, when the two quantities are statistically independent. When the temporal extent of the conjunction is small compared to the orbit period of the objects one can consider the motion of the two objects of S_1 and S_2 as uniform rectilinear with deterministically known velocities $\overline{V}_1$ and $\overline{V}_2$, and compute the collision probability as a two-dimensional integral on the collision b-plane. To this end we define the S_2-centered b-plane reference system $\langle\xi,\zeta,\varsigma\rangle$ with Chan (2008):

$$\bar{u}_\xi = \frac{\overline{V}_1\times\overline{V}_2}{|\overline{V}_1\times\overline{V}_2|}, \qquad \bar{u}_\zeta = \frac{\overline{V}_1 - \overline{V}_2}{|\overline{V}_1 - \overline{V}_2|}, \qquad \bar{u}_\varsigma = \bar{u}_\xi\times\bar{u}_\zeta \tag{23}$$

Under the rectilinear approximation the volume becomes a cylinder along the ζ axis and Eq. (21) can now be written in $\langle\xi,\zeta,\varsigma\rangle$ axes and integrated for $-\infty \le \zeta \le +\infty$ to yield:

$$\begin{aligned} P = \int_A \frac{1}{2\pi\sigma_\xi\sigma_\varsigma\sqrt{1-\rho_{\xi\varsigma}^2}}\exp\Bigg\{-\Bigg[&\left(\frac{\xi-\xi_e}{\sigma_\xi}\right)^2 + \left(\frac{\varsigma-\varsigma_e}{\sigma_\varsigma}\right)^2 \\ &- 2\rho_{\xi\varsigma}\frac{(\xi-\xi_e)}{\sigma_\xi}\frac{(\varsigma-\varsigma_e)}{\sigma_\varsigma}\Bigg]/2(1-\rho_{\xi\varsigma}^2)\Bigg\}d\xi d\varsigma \end{aligned} \tag{24}$$

where $r_m = \langle \xi, 0, \varsigma \rangle$ is the expected closest approach relative position in b-plane axes, A is a circular domain of radius SA and $\sigma_\xi, \sigma_\varsigma, \rho_{\xi\varsigma}$ can be extracted from the relative position of covariance matrix in b-plane:

$$C_{\xi\varsigma} = \begin{pmatrix} \sigma_\xi^2 & \rho_{\xi\varsigma}\sigma_\xi\sigma_\varsigma \\ \rho_{\xi\varsigma}\sigma_\xi\sigma_\varsigma & \sigma_\varsigma^2 \end{pmatrix} \tag{25}$$

The computation of Eq. (24) can be made equivalent to integrating a properly scaled isotropic Gaussian distribution function over an elliptical cross-section. If that cross section is approximated as a circular one of equal area, the final computation of the impact probability reduces to a Rician integral that can be computed with the convergent series Chan (2008):

$$P(u,z) = e^{-z/2}\sum_{m=0}^{\infty}\frac{z^m}{2^m m!}\left(1 - e^{-u/2}\sum_{k=0}^{m}\frac{u^k}{2^k k!}\right) \tag{26}$$

with

$$u = \frac{S_A^2}{\sigma_\xi\sigma_\varsigma\sqrt{1-\rho_{\xi\varsigma}^2}} \tag{27}$$

$$z = \left(\frac{\xi_e}{\sigma_\xi}\right)^2 + \left(\frac{\varsigma_e}{\sigma_\varsigma}\right)^2 - 2\rho_{\xi\varsigma}\frac{\xi_e}{\sigma_\xi}\frac{\varsigma_e}{\sigma_\varsigma} \tag{28}$$

From the above equations it appears that the collision probability is constant when the impact point (ξ_e, ς_e) belongs to an ellipse of semi-axes ratio $\frac{\sigma_\xi}{\sigma_\varsigma}$ and rotated by an angle:

$$\Theta = \frac{1}{2}tan^{-1}\left(\frac{2\rho_{\xi\varsigma}\sigma_\xi\sigma_\varsigma}{\sigma_\xi^2 - \sigma_\varsigma^2}\right) \tag{29}$$

In addition, the collision probability decreases exponentially for increasing z, i.e., as the size of the ellipse increase.

Suppose a direct collision $(\xi_e = 0, \varsigma_e = 0)$ is predicted when the object S_1 has orbital true anomaly υ_c, radial orbital distance r_c and eccentricity e. Let the velocity of S_2 at collision related to the velocity of S_1 by a positive rotation angle $-\pi < \vartheta < \pi$ around S_1 orbital plane normal u_{h1} Bombardelli et al. (2014):

$$\vartheta = \tan^{-1}\left[\frac{(\overline{V}_1 \times \overline{V}_2)\cdot u_{h1}}{\overline{V}_1 \cdot \overline{V}_2}\right] \tag{30}$$

followed by an out of plane rotation $\frac{-\pi}{2} < \Psi < \frac{\pi}{2}$ in the direction approaching u_{h1}:

$$\Psi = \tan^{-1}\left[\frac{(\bar{v}_2 \cdot \bar{u}_h)|\bar{v}_2 \times \bar{u}_h|}{\bar{v}^2 - (\bar{v}_2 \cdot \bar{u}_h)^2}\right] \tag{31}$$

Assuming that a laser impulse $\Delta\overline{V}$ with radial, transverse and out of plane components as follows:

$$\Delta V_r = |\Delta\overline{V}|\cos\gamma\sin(\sigma + \alpha) \tag{32}$$

$$\Delta V_\upsilon = |\Delta\overline{V}|\cos\gamma\cos(\sigma + \alpha) \tag{33}$$

$$\Delta V_h = |\Delta\overline{V}|\sin\gamma \tag{34}$$

where α is the flight path angle of S_1, σ is the in-plane rotation angle, γ is the subsequent rotation angle in the out. After applying maneuver impulse $|\Delta\overline{V}|$ which performed at an angular distance $\Delta v = \upsilon_c - \upsilon_m$, a b-plane shift $\Delta r_m = (\Delta\xi, \Delta\zeta, \Delta\varsigma)$ is resulted:

$$\Delta r_m = RKD|\Delta\overline{V}| = M|\Delta\overline{V}| \tag{35}$$

$$R = \begin{pmatrix} 0 & 0 & -1 \\ \cos\beta & -\sin\beta & 0 \\ -\sin\beta & -\cos\beta & 0 \end{pmatrix} \tag{36}$$

$$K = \begin{pmatrix} \frac{-V_1\sqrt{\mu}}{R_c} & \sin\alpha\sin\upsilon_c & 0 \\ 0 & -\cos\alpha & 1 \\ 0 & \cos\alpha & 1 \end{pmatrix} \tag{37}$$

$$D = \sqrt{\frac{R_c^3}{\mu}}\begin{pmatrix} c_{tr} & c_{t\upsilon} & 0 \\ c_{rr} & c_{r\upsilon} & 0 \\ 0 & 0 & c_{wh} \end{pmatrix} \tag{38}$$

In the above equations β represents the angle between $\overline{V_1}$ and $\overline{V_2}$, μ is the Earth gravitational constant and α is the flight path angle of S_1. The terms c_{tr}, $c_{t\upsilon}$, c_{rr}, $c_{r\upsilon}$, c_{wh} are nondimensional functions of e, υ_c and υ_m provided in Bombardelli (2014) and Bombardelli et al. (2014).

3. Numerical application

With the intention of maximize engagement opportunities to illuminate debris in sun-synchronous orbits, the location is chosen to be as close as possible to the poles. Moreover, high altitude reduces the atmospheric beam losses and turbulence effects. The ideal site would be the PLATeau Observatory (PLATO) at Dome A in Antarctica, which is at 4 km altitude, latitude of 81°S and longitude of 72°E Mason et al. (2011). The typical Sun-synchronous orbits have about 600-800 km altitude, with periods in the range of 96–100 min, and inclinations of around 98° Rosengren (1992). The laser force is calculated under the following postulates:

1. The radiation fall normal to the debris surface (i.e., $\eta = 0$) as the debris crossing its perigee.
2. The debris surface is considered to be perfectly reflecting surface. So, the laser force will be duplicated, where the surface specularity $\beta = 1$ and surface reflectivity $\rho' = 1$. While the absorption coefficient $\alpha' = 0$.

As a first step, the laser scheme is applied on debris of known mass and area. A discarded lens cap from the Japanese Akari IR space telescope was chosen as the demonstration object (U.S. Catalog ID: 29054) where its area to mass ratio is ~0.04 (kg/m^2) Mason et al. (2011). On 02 January 2014, the object has the following two line elements (Table 1):

For the chosen location, the rising and setting times of the debris are calculated using Satellite Tracking Software: Pass

Table 1 Debris two line element.

1	29054U	06005E	14002.16916607	.00001553	00000-0	34531-3 0 2417	
2	29054	98.2356	10.3600	0010523	50.2050	310.0074	14.58342766417977

Table 2 Average of orbital velocity change over different intervals.

Time interval	Average $\lvert\Delta\overline{V}\rvert$ (cm/s)
Per second	0.2
After one revolution	0.4
After one day	2.6

Table 3 Encounter geometry.

a (Km)	E	β	υ_e
7155.8	5×10^{-4}	40°	18°

Scheduler version 1.50 by Kelso (1999). For elevation of 10°, the average transit time is about 7 min. One debris revolution is nominally chosen for simulations in which the rising and setting times are 11.8111 UT and 11.9217 UT respectively which are corresponded to mean anomalies $\mathbf{M_{rise}} = \mathbf{45.094}^{\circ}$ and $\mathbf{M_{set}} = \mathbf{45.5161}^{\circ}$. Using Newton iteration, the eccentric anomalies for rising and setting are $\mathbf{E_{rise}} = \mathbf{45.1277}^{\circ}$ and $\mathbf{E_{set}} = \mathbf{45.5499}^{\circ}$. Consequently, the true anomalies for rising and setting are $\upsilon_{\mathbf{rise}} = \mathbf{65.6822}^{\circ}$ and $\upsilon_{\mathbf{set}} = \mathbf{89.8755}^{\circ}$ which are considered as the bounds of the integral given by Eq. (13). The orbital velocity change due to laser force for one revolution is illustrated in the following graphs:

It is illustrated that the mean $\lvert\Delta\overline{V}\rvert$ due to laser force is about 0.2 cm/s which can be accumulated and grow over time as illustrated in the following table:

For one revolution, the relation of orbital velocity change with both eccentricity and area to mass ratio when the object passes through perigee point are investigated in the following figures:

Consider a hypothetical collision between two objects S_1 and S_2 with $\varsigma_e = 100m$ and $\xi_e = 0$ the encounter geometry is summarized in Table 2 (see Table 3).

In addition we assume a 5 m spherical envelope for S_1 and 4 m spherical envelope for S_2. For both object, it is assumed that a diagonal covariance matrix is:

$$C_{\xi\varsigma} = \begin{pmatrix} 0.03\ \text{km}^2 & 0 \\ 0 & 0.6\ \text{km}^2 \end{pmatrix}$$

Consider a fully tangential laser impulse (i.e., $\sigma = \gamma = 0$) corresponds to 0.2 cm/s laser $\lvert\Delta\overline{V}\rvert$ over one revolution and grow with time. The b-plane shift Δr_m is illustrated in the following figures: (see Figs. 2–3b).

As shown in Fig. 4, the miss distance shift increases as the angular distance increase with an average of about 30 km over an angular distance of 2π (Fig. 4a) which can be grown over time with an average of 58 km over an angular distance 6π (Fig. 4b). The collision probability change is illustrated in the following figure:

As shown in Fig. 5, the collision probability decreases as the angular distance increase with an average of about 2.9×10^{-4} over an angular distance of 2π (Fig 5a) which can be reduced over time with an average of 2.75×10^{-4} over an angular distance of 6π (Fig. 5b).

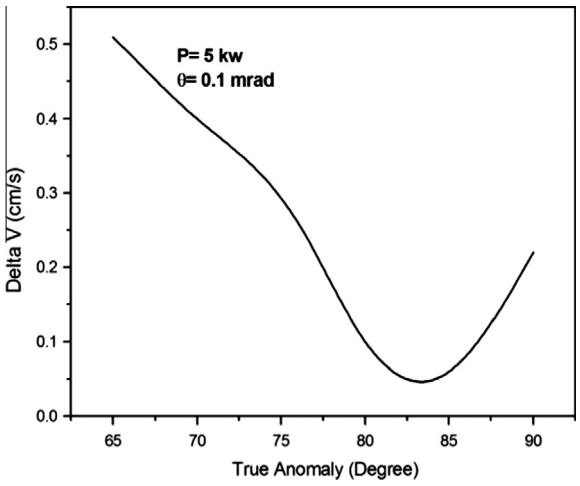

Figure 2 Velocity change $\lvert\Delta\overline{V}\rvert$ over the transit time for one orbital revolution.

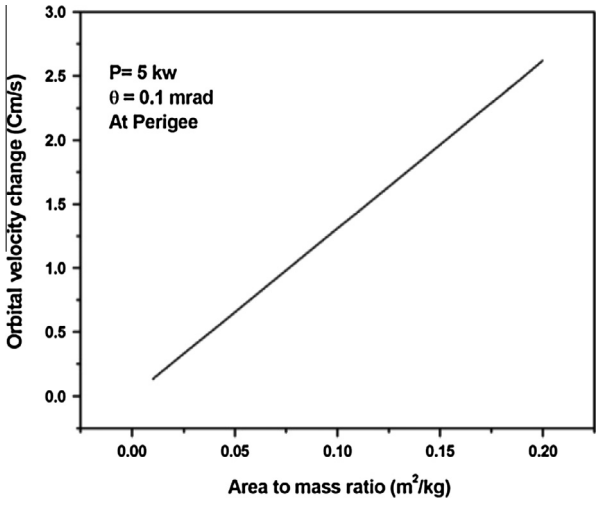

Figure 3a Orbital velocity change due to the laser force for different eccentricity.

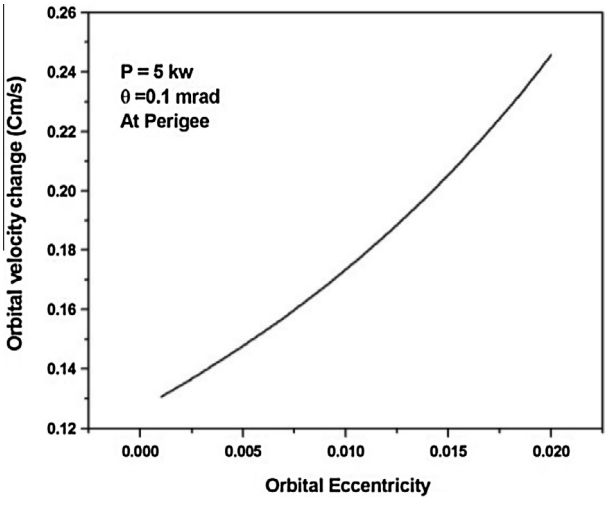

Figure 3b Orbital velocity change due to the laser force for different area to mass ratio.

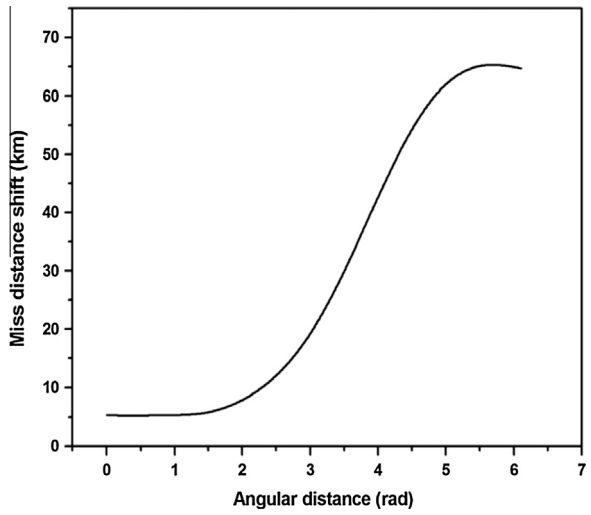

Figure 4a Miss distance shift over an angular distance for one revolution.

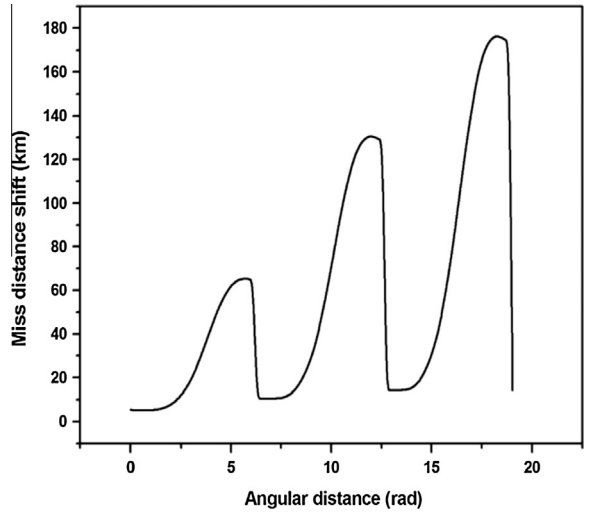

Figure 4b Miss distance shift grow over time.

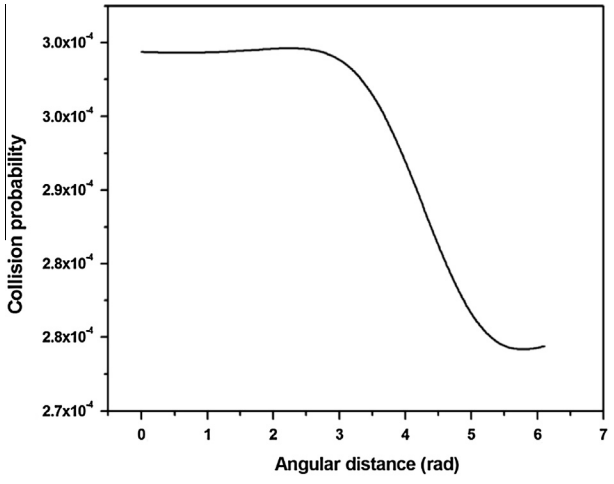

Figure 5a Collision probability over an angular distance for one revolution.

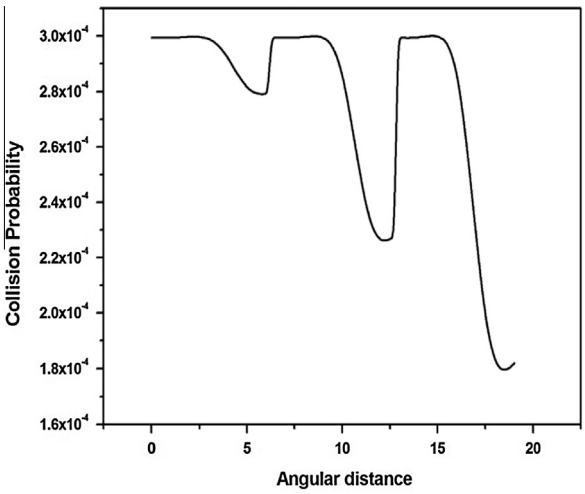

Figure 5b Collision probability over time.

4. Conclusion

A simple analytical formulation of using ground based laser force for collision avoidance of LEO objects has been presented. It has been verified that medium power laser of about 5 kW resulted in an orbital velocity change $|\Delta\overline{V}|$ with an average of 0.2 cm/s which depends directly on the orbital eccentricity in addition to area to mass ratio. Over time, $|\Delta\overline{V}|$ is growing to be about 3 cm/day which consequently results in perturbing the semi-major axis, increasing the miss distance and decreasing the collision probability of the approaching objects. So, it can be concluded that ground based laser can be used for debris collision avoidance.

References

Bombardelli, Claudio, 2014. Analytical formulation of impulsive collision avoidance dynamics. Celest. Mech. Dyn. Astron. 118.

Bombardelli, Claudio, Hernando-Ayuso, Javier, García-Pelayo, Ricardo, 2014. Collision avoidance maneuver optimization. Adv. Astronaut. Sci. AAS14-335.

Campbell, Jonathan W., 2000. Colonel, USAFR, Using Lasers in Space Laser Orbital Debris Removal and Asteroid Deflection, Center for Strategy and Technology Air War College Occasional Paper No. 20, 2000.

Chan, F.K., 2008. Spacecraft Collision Probability. Aerospace Press.

Choi, Sang H., Pappa, Richard S., 2012. Assessment study of small space debris removal by laser satellites. Recent Progr. Space Technol. 2 (2).

Danielson, E., Levin, J., Abrams, E., 2003. Meteorology, second ed. McGraw-Hill Companies.

El-Saftawy, M.I., Abd El-Hameed, Afaf M., Khalifa, N.S., 2007. Analytical Studies of Laser Beam Propagation through the Atmosphere, In: Proceeding of 6th International Conference on Laser Science and Applications (ICLAS-07), Cairo, Egypt.

Escobal, P.R., 1965. Methods of Orbit Determination. John Wiley and Sons Inc., New York, London, Sydney.

Kelso, T.S., 1999. Pass scheduler version 1.50. Satellite Tracking Software.

Khalifa, N.S., 2009. Effect of an Artificial Radiant Force on the Spacecraft's Orbit. Phd. Thesis, Cairo university.

Mason, James, Stupl, Jan, Marshall, William, Levit, Creon, 2011. Orbital debris–debris collision avoidance. Adv. Space Res. 48.

Mc Innes Colin, R., 1999. Solar Sailing: Technology, Dynamics and Mission Applications. Springer–Praxis Series in Space Science and Technology.

Phipps, Claude R., Baker, Kevin L., Libby, Stephen B., Liedahl, Duane A., Olivier, Scot S., pleasance, Lyn D., Rubenchik, Alexander, Trebes, James E., Victor George, E., Marcovici, Bogdan, Reilly, James P., Valley, Michael T., 2012. Removing orbital debris with pulsed lasers. AIP Conf. Proc. 1464.

Rosengren, M., 1992. ERS-1 – an earth observer that exactly follows its chosen path. ESA Bull. 72.

Roy, A.E., 1978. Orbital Motion. Adam Hilger Ltd., Bristol.

Stupl, Jan, Mason, James, Marshall, William, Levit, Creon, 2010. Debris–Debris Collision Avoidance Using Medium Power Ground-Based Lasers, Beijing Orbital Debris Mitigation Workshop. Beihang University, Beijing, People's Republic of China.